Onsets and spectra of impulsive solar energetic electron events observed near the Earth

Eduard P. Kontar and Hamish A. S. Reid

Department of Physics and Astronomy, University of Glasgow, G12 8QQ, United Kingdom

eduard@astro.gla.ac.uk, hamish@astro.gla.ac.uk

ABSTRACT

Impulsive solar energetic electrons are often observed in the interplanetary space near the Earth and have an attractive diagnostic potential for poorly understood solar flare acceleration processes. We investigate the transport of solar flare energetic electrons in the heliospheric plasma to understand the role of transport to the observed onset and spectral properties of the impulsive solar electron events. The propagation of energetic electrons in solar wind plasma is simulated from the acceleration region at the Sun to the Earth, taking into account self-consistent generation and absorption of electrostatic electron plasma (Langmuir) waves, effects of non-uniform plasma, collisions and Landau damping. The simulations suggest that the beam-driven plasma turbulence and the effects of solar wind density inhomogeneity play a crucial role and lead to the appearance of a) spectral break for a single power-law injected electron spectrum, with the spectrum flatter below the break, b) apparent early onset of low-energy electron injection, c) the apparent late maximum of low-energy electron injection. We show that the observed onsets, spectral flattening at low energies, and formation of a break energy at tens of keV is the direct manifestation of wave-particle interactions in non-uniform plasma of a single accelerated electron population with an initial power-law spectrum.

Subject headings: Sun: flares - Sun: X-rays, gamma rays - Sun: activity -Sun: particle emission

1. Introduction

Solar flares are extremely efficient at accelerating electrons to non-thermal energies, which can subsequently be observed either by their emission at X-ray and radio wavelengths or escaping along open magnetic field lines via direct electron measurements near

the Earth (see Aschwanden 2002; Brown & Kontar 2005; Benz 2008, for a review). The first in-situ observations of energetic particles (van Allen & Krimigis 1965) opened up the non-electromagnetic window of flare accelerated particle observations. Solar impulsive electron events detected in-situ generally display broken power-law energy distributions with lower energies having softer spectra (Lin 1985). These events also show near time-of-flight velocity dispersion and a beamed pitch-angle distribution (e.g. Lin 1985; Krucker et al. 1999, 2007). From this evidence, it is often believed that such electrons propagate scatter-free from the Sun to the Earth (e.g. Wang et al. 2006). The observed correlation between the spectral indices of energetic electrons at the Sun from X-ray data and the Earth from in-situ data (Lin 1985; Krucker et al. 2007) is often viewed as an additional support for this model. At the same time, impulsive solar energetic electron events are closely related observationally (e.g. Lin et al. 1981; Ergun et al. 1998; Gosling et al. 2003; Cane 2003; Krucker et al. 2007) and theoretically (Ginzburg & Zhelezniakov 1958; Zaitsev et al. 1972; Grognard 1982; Melrose 1990; Melnik et al. 1999; Kontar 2001a; Ledenev et al. 2004) to Type III solar radio bursts.

The standard model of Type III solar radio bursts (Ginzburg & Zhelezniakov 1958) suggests that electron beams propagating in the ambient solar wind plasma from the Sun to the Earth can excite Langmuir waves, which in turn generate escaping plasma radio emission (see Melrose 1985, for a review). In a one-dimensional treatment assuming travel along magnetic field lines, as faster electrons outpace slower electrons a positive gradient is formed in velocity space. If this positive gradient gets large enough to start the generation of waves, electron energy is resonantly transferred to Langmuir waves in the background plasma. This transfer of energy reduces the gradient in velocity space forming a plateau (Vedenov et al. 1962; Drummond & Pines 1962). For a spatially limited electron beam cloud, the plasma waves generated at the front of the cloud are absorbed by the electron beam at the back allowing the electrons to travel through the corona with small energy losses and with a velocity that decreases with time due to plasma inhomogeneity (Kontar 2001a). Although this broad picture is often supported by observations, the detailed picture of electron transport and plasma radio emission is far from well-understood. This is largely due to electron beam propagation and radio emission being essentially a non-linear multi-scale problem, and is the subject of a large number of ongoing simulation efforts (e.g. Melnik et al. 1999; Kontar 2001a; Kontar & Pécseli 2002; Ledenev et al. 2004; Li et al. 2006; Gaelzer et al. 2008).

Solar impulsive electron events can span a broad range of energies, from a few keV to hundreds of keV (Lin et al. 1996). Their energy distribution forms a broken power-law spectrum with the break energy in deca-keV range. Despite often showing the near time-of-flight dispersion, lower energy electrons appear to arrive sooner than expected from a scatter-free model (Wang et al. 2006). Since the low energy electrons of a few keV should lose their energy collisionally in the low corona, these electrons are believed to be accelerated

high in the corona (Lin et al. 1996). Recent time-of-injection analysis (Wang et al. 2006) assuming scatter-free propagation of solar energetic electrons suggests the existence of two electron populations, one low energy beam injected before the start of the type III burst and one high energy beam injected after the type III burst.

In this Letter, we investigate the electron propagation from the Sun to the Earth taking into account the scattering of electrons by beam-driven plasma waves. We show, for the first time, that the generation and absorption of Langmuir waves by an electron beam in the non-uniform solar corona leads to the appearance of a break energy in the observed spectrum at the Earth and naturally explains the observed apparent early injection of low energy electrons.

2. Modelling electron propagation in the heliosphere

The transport of energetic electrons in the heliospheric plasma is governed by a variety of different processes (see Melrose 1990, for a review). In this work we consider solar energetic electrons propagating along open magnetic field lines and assume their transport can be described one-dimensionally ignoring electromagnetic effects. Under this assumption, the evolution of the electron distribution function f(v, x, t) [electrons cm⁻⁴ s] and the spectral energy density of electron plasma waves W(v, x, t) [ergs cm⁻²] can be described self-consistently by the following kinetic equations (e.g. Kontar 2001a)

$$\frac{\partial f}{\partial t} + v \frac{\partial f}{\partial x} = \frac{4\pi^2 e^2}{m^2} \frac{\partial}{\partial v} \frac{W}{v} \frac{\partial f}{\partial v}$$
 (1)

$$\frac{\partial W}{\partial t} + \frac{\partial \omega}{\partial k} \frac{\partial W}{\partial x} - \frac{\partial \omega_{pe}}{\partial x} \frac{\partial W}{\partial k} = (\gamma(v, x) - \gamma_c - \gamma_L)W \tag{2}$$

where $\partial \omega/\partial k = 3v_{Te}^2/v$ is the group velocity of Langmuir waves, k is the wavenumber of a Langmuir wave, $\gamma(v,x) = \frac{\pi \omega_{pe}}{n} v^2 \frac{\partial f}{\partial v}$ is the plasma wave growth rate, and γ_c and γ_L are the collisional and Landau damping rates of waves respectively. The first term on the right hand side of both Equation (1) and (2) describes the resonant interaction, $\omega_{pe} = kv$, of electrons and Langmuir waves and was first derived by Vedenov et al. (1962) and Drummond & Pines (1962). W(v,x,t) is normalized to the wave energy density $\int W dk$ [ergs cm⁻³] and plays a similar role for plasma waves as the electron distribution function does for particles.

2.1. Initial electron beam distribution

The initial distribution function is assumed to be a power-law with spectral index α in velocity space and has a finite spatial size d at initial time t = 0:

$$f(v, x, t = 0) = g_o(v) \exp\left(-\frac{x^2}{d^2}\right)$$
(3)

where

$$g_0(v) = n_{beam} \frac{(\alpha - 1)}{v_{min}} \left(\frac{v_{min}}{v}\right)^{\alpha}, \quad \alpha > 1$$
(4)

is the initial electron distribution function normalized to n_{beam} , the beam electron number density, v_{min} is the low velocity cutoff, and α is the spectral index of the initial electron beam. The injected electron flux density differential in energy $F_0(E,x,t=0)$ [electrons cm⁻² keV⁻¹ s⁻¹] is also a power law $F_0(E) \sim E^{-\delta}$, where $\delta = \alpha/2$. The initial spectral energy density of the Langmuir waves is assumed to be thermal $W(v,x,t=0) = k_B T/(2\pi^2 \lambda_D^2)$, where T is the background plasma temperature, k_B is Boltzmann constant and λ_{De} is the electron Debye length.

2.2. Heliospheric plasma density

The background plasma is modelled using a heliospheric density model by Parker (1958) with normalization by Mann et al. (1999) that can be found by numerically integrating the equations for a stationary spherical symmetric solution for solar wind (Parker 1958)

$$r^2 n(r)v(r) = C = const (5)$$

$$\frac{v(r)^2}{v_c^2} - \ln\left(\frac{v(r)^2}{v_c^2}\right) = 4\ln\left(\frac{r}{r_c}\right) + 4\frac{r_c}{r} - 3\tag{6}$$

where $v_c \equiv v(r_c) = (k_B T/\tilde{\mu} m_p)^{1/2}$, $r_c = GM_s/2v_c^2$, T is the electron plasma temperature, M_s is the mass of the Sun. The constant appearing above is fixed by satellite measurements near the Earth's orbit (at r = 1 AU, n = 6.59 cm⁻³) and equates to 6.3×10^{34} s⁻¹.

3. Simulation of electron transport

The system of kinetic equations (1, 2) have been solved using finite difference methods as described in (Kontar 2001a) for a variety of initial beam parameters. The temperature of the heliospheric plasma was taken to be constant at $T = 10^6 K$ and the plasma density

profile is given by the numerical solution of Equations (5, 6). The low velocity cutoff was taken equal to approximately twice the thermal electron velocity $v_{min} = 1.2 \times 10^9$ cm/s. The initial spatial size of the electron cloud was taken as $d = 5 \times 10^9$ cm so the injection time of electrons with velocity 5×10^9 cm/s is one second, which is a typical duration of type III bursts near the starting frequencies (Dulk 1985). The initial beam density n_{beam} was varied from 1×10^{-3} cm⁻³ to 1 cm⁻³ to explain the observed fluxes near the Earth. The fluence spectra of such beam densities correspond to weak to medium solar energetic electron events observed near the Earth and are required for realistic simulation computational times. The initial height of the beam was 5×10^9 cm corresponding to the density 2.1×10^9 cm⁻³ (local plasma frequency ~ 415 MHz). The initial beam spectral indices $\delta = \alpha/2$ were between 2.5 and 4.5, consistent with the observational values Krucker et al. (2009).

3.1. Electron spectra at 1AU

Generally, it is seen from our simulations that as soon as the plasma wave growth time $\sim 1/\gamma(v,x)$ is less than the time scale of an electron cloud d/v for some energy E(v), the wave-particle interactions start to play an important role in the electron transport. Since this condition is energy dependent the electrons above certain energies are too dilute to generate plasma waves. The overall spectrum observed at the Earth becomes close to a broken power-law, where electrons below the break energy generate and absorb Langmuir waves, while electrons above the break energy are not affected by the wave-particle interactions.

Traditionally in-situ measurements of energetic electrons (e.g. Lin et al. 1995) provide the flux density differential in energy F(E,x,t)=f(v,x,t)/m [electrons cm⁻² s⁻¹ keV⁻¹] and the fluences (flux integrated over the duration of an event) [electrons cm⁻² keV⁻¹]. The injected electron fluence in our model $\int_{-\infty}^{\infty} f(v,x,t)/vdx$ can be calculated from equations (3,4) and is presented in Figure 1. The corresponding energy spectral index of the injected electron fluence at the Sun is $(\alpha+1)/2=\delta+1/2$. The resulting spectrum of solar energetic particles at the Earth is also presented in Figure 1. As can be seen from Figure 1, the spectrum of energetic particles above the break ~ 35 keV is identical to the spectrum of injected electrons so we can deduce these particles have indeed propagated scatter-free (in our model). The particles below the break energy do not propagate freely but generate electron plasma waves. The beam generated plasma waves drift in velocity-space toward lower phase velocities due to the solar wind density gradient (Kontar 2001a). This drift, caused by the decreasing ambient plasma density, takes waves out of resonance with the particles which generated them and so reduces the wave energy at a given point in phase space. At lower phase velocities these waves can be more easily absorbed by the thermal

plasma via Landau damping. Therefore, particles arriving later to this point in phase space are unable to restore the injected spectrum because they cannot absorb the same amount of energy from the waves. This results in a flatter energy spectrum of electrons below some energy where beam-plasma interactions are important (Figure 1).

3.2. Break energies and spectral indices

We note the spectrum below the break is not exactly a power-law although resembles one closely, therefore to compare with observations, which have normally poor energy resolution $\Delta E \sim 0.1E$ (e.g. Lin et al. 1995), we fitted our simulated spectra with simple power-law fits. The spectral index below the break energy δ_{low} is always smaller than the spectral index above the break energy δ_{high} and correlates (Figure 2) with δ_{high} in a remarkably similar manner as observed by Krucker et al. (2009). The range of δ_{low} appear in a rather narrow range between 2 and 2.5 for a wide range of injected spectral indices between 3 and 5 (Figure 2). The actual value of δ_{low} is also dependent on the background plasma density and will be different should the heliospheric density model change.

The break energy range for all simulations is between 4 keV and 80 keV (Figure 2), with the exact break energy being dependent on the initial spectral index of the beam, δ_{high} , and the initial density of the beam. As the initial density of the beam increases, the break of spectral index occurs at higher energies. Indeed, the larger number of injected electrons, the faster the generation of plasma waves proceeds and hence the stronger the interaction between electrons and plasma waves. This also explains the dependence of break energy to the injected spectral index, with lower spectral indices having a larger population of higher energy electrons and hence having higher break energies. The fluence at the break energy correlates to the break energy itself (Figure 2) with higher break energies corresponding to lower fluence magnitudes.

3.3. Electron time-of-flight and apparent injection time

The particles arriving at the Earth (1.2 AU) show near time-of-flight dispersion (Figure 3), often observed by satellites in impulsive solar electron events. Assuming scatter-free propagation, i.e. without any interaction with plasma, one can produce the apparent injection profile at the Sun, as Krucker et al. (1999); Wang et al. (2006) did for observations. Under scatter-free assumption, the time-of-flight for energetic electrons from the Sun to the spacecraft is simply $t_A = L/v(E)$, where L = 1.2 AU is the distance and v(E) is the speed of

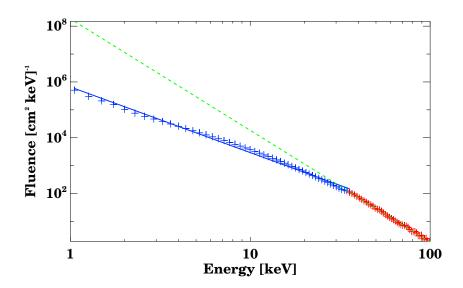


Fig. 1.— The simulated spectrum (fluence [electrons cm⁻² keV⁻¹]) of solar flare energetic particles at the Earth (crosses). The blue (red) line shows the power law fit to the spectrum below (above) the break energy 35 keV. The green line shows the initially injected fluence. Spectral index of injected electrons is $\delta_{high} = 4$. The spectral index below the break is $\delta_{low} = 2.35$.

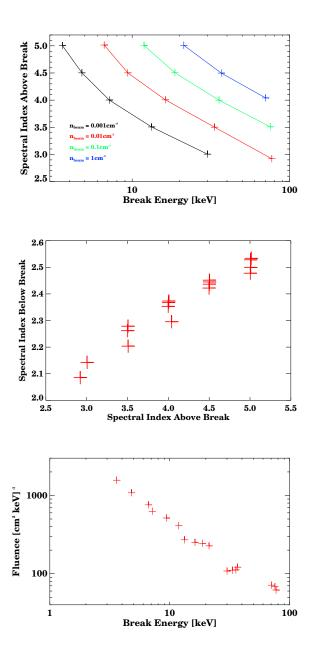


Fig. 2.— Top: Spectral index above the break δ_{high} versus break energy for various electron densities and spectral indices; Middle: Spectral index below the break δ_{low} energy versus spectral index above the break energy; Low: Fluence at the break energy versus break energy. Note that the simulations have been done for different particle densities and different spectral indices as given in the top panel.

electrons for various energies. The time of arrival is then simply $t_A = t_{inj} + L/v(E)$, where t_{inj} is the apparent injection time. These apparent injection profiles with background added have been calculated from the simulated fluxes at 1.2 AU (see Figure 4). If the electrons propagate scatter-free they would require 10-20 minutes earlier onset of injection t_{inj} of low (3-12 keV) energy electron injection and a delayed maximum of the injection to explain observations. An identical simulation was ran with an electron beam not interacting with the background plasma (scatter free propagation) and the results are compared in Figure 4. Comparing the calculated injection profiles over various energies one observes good agreement between free-streaming and full simulations at energies above the break energy 35 keV. The apparent injection profile at lower energies becomes wider than the free streaming case, and 3-25 keV electrons show apparent early injection of 1 - 20 minutes before the actual injection. The lower energy is, the earlier the apparent onset of the injection. The low energy electrons at the Earth are not only due to the injection at the Sun but because of the in-flight deceleration of faster particles. These electrons had initial energy higher than the detected energy at 1.2 AU, hence they have traveled a part of the distance faster than can be inferred from their detected energies. The relaxation of the electron distribution function towards a flatter shape in velocity space $\partial f(v,x,t)/\partial v \sim 0$ means at a specific spatial location, some electrons have energies too low to have arrived by free propagation alone. In addition, the maximum of apparent injection profile at energies below $\sim 35 \text{ keV}$ appears later. Therefore, the similar injection profile obtained (Wang et al. 2006) should be interpreted as the direct evidence of electron plasma wave scattering in the heliosphere and not the indication of a separate acceleration mechanism. This early injection time is a direct result of low-energy electron driven turbulence in non-uniform plasma, which affects the propagation of electrons. As evident from Figure 4, the onset of electron injection is also instrument background dependent - the higher/lower background levels would lead to later/earlier injection times for low energy electrons.

4. Discussion and Conclusions

The generation and reabsorption of electron plasma waves by the electron beam in a non-uniform plasma plays an important role in the electron transport and should be taken into account when in-situ electron measurements are analyzed and interpreted. The simulations presented successfully reproduce the spectral and temporal characteristics of observed solar energetic electron events. The scattering of the solar energetic particles by the beam-driven electrostatic plasma waves leads to the appearance of a broken power-law in energy spectrum, and the apparent early injection of low energy electrons in a few keV range at the Sun. We emphasize here that it is the combined effect of plasma wave generation and non-uniform

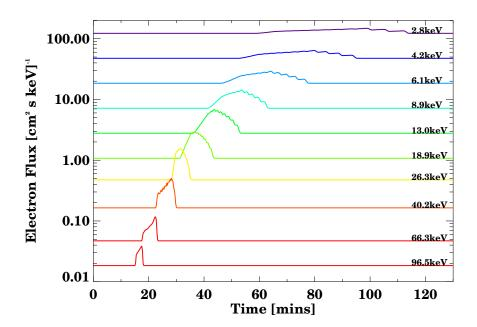


Fig. 3.— Simulated electron flux density time profiles of energetic electrons for WIND/3DP energies (Lin et al. 1995). Electron flux density [electrons cm⁻² s⁻¹ keV⁻¹] as a function of time at 1.2 AU for 10 energy channels. The time t=0 corresponds to the injection time at the Sun. The sawtooth structure appearing in low energy channels is an artifact of finite binning in the velocity space. The initial beam parameters are the same as in Figure 1.

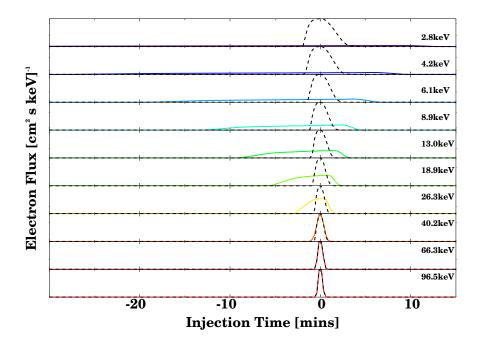


Fig. 4.— The apparent injection profiles of electrons at the Sun *assuming* free streaming of all electrons. The plotted fluxes are normalized to the maxima of the scatter free case. The injection profiles for scatter-free propagation (without generation and absorption of waves) is overplotted with dashed lines. The initial beam parameters are the same as in Figure 3.

density inhomogeneity that leads to the appearance of a broken power-law.

We have shown that the low energy electrons (below the break) are originally injected with higher energies but have lost some their energy to plasma waves in the background plasma and are therefore detected earlier than their energy at the spacecraft suggest. The apparent early start of low energy electron injection appears due to propagation effects and does not require a secondary beam population (c.f. Wang et al. 2006). Moreover, the simulations naturally explain the linear correlation between low energy and high energy spectral indices often observed in the spectra of solar impulsive electron events (Krucker et al. 2009).

The characteristic time of beam-plasma interaction via electron plasma waves is inversely proportional to the density of the energetic electrons. If the beam is dilute, electrons do not generate plasma turbulence and the spectrum of such electrons could be free from propagation effects (in our model). Such events are likely to be seen only at low energies (e.g. Krucker et al. 2009). If the beam is dense enough to excite Langmuir waves, the initially injected power-law spectrum will be detected as a broken power-law. The break energy is dependent on a number of parameters: spectral index of injected solar electrons, the density of the energetic electrons, and the heliospheric density model. Therefore, the correlation between break energy and fluence at the break energy should be taken with care. Our simulations also suggest that in order to deduce meaningful time-of-flight parameters (e.g. injection times), the energetic electrons should be always analyzed in the channels above the break energy and not above some fixed energy as sometimes done in the literature.

While our simulations can successfully explain and reproduce a number of observed properties and highlight the governing role of wave-particle interactions at keV- tens of keV energies, the heliospheric plasma - electron beam system is more complex. First, the different density models (e.g. Newkirk 1967; Saito et al. 1977) could change the break energy values, although will not alter the overall conclusions. Second, the heliospheric plasma has density perturbations on various scales which can affect the evolution of plasma waves (Kontar & Pécseli 2002), lead to a spiky structure of the Langmuir waves (Melrose 1990; Kontar 2001b; Li et al. 2006), often observed in the interplanetary space (Lin 1985), and hence affect the electron distribution. In addition, the higher energy solar impulsive electron events demonstrate injection with ~ 10 min delay after the onset of type III bursts (e.g. Krucker et al. 1999; Haggerty & Roelof 2002). Therefore, additional simulations and in-situ measurements are needed to understand this complex non-linear system.

EPK acknowledges financial support of STFC rolling grant and STFC/PPARC Advanced Fellowship. Financial support by the European Commission through the SOLAIRE

Network (MTRN-CT-2006-035484) is gratefully acknowledged.

REFERENCES

Aschwanden, M. J. 2002, Space Science Reviews, 101, 1

Benz, A. O. 2008, Living Reviews in Solar Physics, 5, 1

Brown, J. C., & Kontar, E. P. 2005, Advances in Space Research, 35, 1675

Cane, H. V. 2003, ApJ, 598, 1403

Drummond, W. E., & Pines, D. 1962, Nucl. Fusion Suppl., 3, 1049

Dulk, G. A. 1985, ARA&A, 23, 169

Ergun, R. E., Larson, D., Lin, R. P., McFadden, J. P., Carlson, C. W., Anderson, K. A., Muschietti, L., McCarthy, M., Parks, G. K., Reme, H., Bosqued, J. M., D'Uston, C., Sanderson, T. R., Wenzel, K. P., Kaiser, M., Lepping, R. P., Bale, S. D., Kellogg, P., & Bougeret, J.-L. 1998, ApJ, 503, 435

Gaelzer, R., Ziebell, L. F., Viñas, A. F., Yoon, P. H., & Ryu, C.-M. 2008, ApJ, 677, 676

Ginzburg, V. L., & Zhelezniakov, V. V. 1958, Soviet Astronomy, 2, 653

Gosling, J. T., Skoug, R. M., & McComas, D. J. 2003, Geophys. Res. Lett., 30, 130000

Grognard, R. J.-M. 1982, Sol. Phys., 81, 173

Haggerty, D. K., & Roelof, E. C. 2002, ApJ, 579, 841

Kontar, E. P. 2001a, Sol. Phys., 202, 131

—. 2001b, A&A, 375, 629

Kontar, E. P., & Pécseli, H. L. 2002, Phys. Rev. E, 65, 066408

Krucker, S., Kontar, E. P., Christe, S., & Lin, R. P. 2007, ApJ, 663, L109

Krucker, S., Larson, D. E., Lin, R. P., & Thompson, B. J. 1999, ApJ, 519, 864

Krucker, S., Oakley, P. H., & Lin, R. P. 2009, ApJ, 691, 806

Ledenev, V. G., Zverev, E. A., & Starygin, A. P. 2004, Sol. Phys., 222, 299

Li, B., Robinson, P. A., & Cairns, I. H. 2006, Physical Review Letters, 96, 145005

Lin, R. P. 1985, Sol. Phys., 100, 537

Lin, R. P., Anderson, K. A., Ashford, S., Carlson, C., Curtis, D., Ergun, R., Larson, D., McFadden, J., McCarthy, M., Parks, G. K., Rème, H., Bosqued, J. M., Coutelier, J., Cotin, F., D'Uston, C., Wenzel, K.-P., Sanderson, T. R., Henrion, J., Ronnet, J. C., & Paschmann, G. 1995, Space Science Reviews, 71, 125

Lin, R. P., Larson, D., McFadden, J., Carlson, C. W., Ergun, R. E., Anderson, K. A., Ashford, S., McCarthy, M., Parks, G. K., Rème, H., Bosqued, J. M., d'Uston, C., Sanderson, T. R., & Wenzel, K. P. 1996, Geophys. Res. Lett., 23, 1211

Lin, R. P., Potter, D. W., Gurnett, D. A., & Scarf, F. L. 1981, ApJ, 251, 364

Mann, G., Jansen, F., MacDowall, R. J., Kaiser, M. L., & Stone, R. G. 1999, A&A, 348, 614

Melnik, V. N., Lapshin, V., & Kontar, E. 1999, Sol. Phys., 184, 353

Melrose, D. B. 1985, Plasma emission mechanisms (Solar Radiophysics: Studies of Emission from the Sun at Metre Wavelengths), 177–210

—. 1990, Sol. Phys., 130, 3

Newkirk, G. J. 1967, ARA&A, 5, 213

Parker, E. N. 1958, ApJ, 128, 664

Saito, K., Poland, A. I., & Munro, R. H. 1977, Sol. Phys., 55, 121

van Allen, J. A., & Krimigis, S. M. 1965, J. Geophys. Res., 70, 5737

Vedenov, A. A., Lelikhov, E. P., & Sagdeev, R. Z. 1962, Nucl. Fusion Suppl., 2, 465

Wang, L., Lin, R. P., Krucker, S., & Gosling, J. T. 2006, Geophys. Res. Lett., 33, 3106

Zaitsev, V. V., Mityakov, N. A., & Rapoport, V. O. 1972, Sol. Phys., 24, 444

This preprint was prepared with the AAS IATEX macros v5.2.